

Enhanced Static Approximation to the Electron Self-Energy Operator for Efficient Calculation of Quasiparticle Energies

Wei Kang and Mark S. Hybertsen

Center for Functional Nanomaterials,

Brookhaven National Laboratory, Upton, NY 11973

(Dated: August 26, 2010)

Abstract

An enhanced static approximation for the electron self energy operator is proposed for efficient calculation of quasiparticle energies. Analysis of the static COHSEX approximation originally proposed by Hedin shows that most of the error derives from the short wavelength contributions of the assumed adiabatic accumulation of the Coulomb-hole. A wavevector dependent correction factor can be incorporated as the basis for a new static approximation. This factor can be approximated by a single scaling function, determined from the homogeneous electron gas model. The local field effect in real materials is captured by a simple ansatz based on symmetry consideration. As inherited from the COHSEX approximation, the new approximation presents a Hermitian self-energy operator and the summation over empty states is eliminated from the evaluation of the self energy operator. Tests were conducted comparing the new approximation to GW calculations for diverse materials ranging from crystals and nanotubes. The accuracy for the minimum gap is about 10% or better. Like in the COHSEX approximation, the occupied bandwidth is overestimated.

PACS numbers: 71.15.Qe 71.10.-w 73.22.-f

I. INTRODUCTION

Understanding the electronic excitation energies of a material system is fundamental to a broad array of material properties. Formally, these correspond to the spectra associated with electron removal and electron addition. In practice, the electronic excitations are the starting point for understanding many phenomena, e.g. through the density of states at the Fermi energy of a metal, the minimum energy gap and associated band effective masses in a semiconductor or the frontier energy levels in a nanoscale junction that control electron tunneling. While the electronic excitation energies can be very often interpreted within an independent electron picture, the many-body treatment of the electron-electron interaction remains fundamental to the predictive calculation of the quasiparticle energies¹. Density functional theory (DFT)^{2,3} has been widely successful in the prediction of the ground-state derived properties of a wide array of materials systems. However, the corresponding effective single particle eigenvalues that emerge from the Kohn-Sham equations are not generally justified to be interpreted as quasiparticle energies and in practice there are significant errors such as the substantial underestimation of semiconductor band gaps⁴. In a many-body perturbation theory approach, the central quantity in the theory is the non-local, energy dependent electron self energy operator. The GW approximation for the electron self energy introduced by Hedin⁵ has been widely exploited for predictive calculations of quasiparticle energies in real materials⁶⁻⁸.

The substantial extra complexity associated with calculating the non-local, energy dependent self energy operator and then using it to solve for quasiparticle properties inspired early efforts to find simplifying approximations, for example the local approximation suggested by Sham and Kohn⁹ and the static COHSEX approximation of Hedin⁵. However, since the first successful implementations for real materials¹⁰⁻¹² it has been clear that both non-locality and energy dependence of the self energy operator play an essential role for accurate results. Subsequently GW calculations have been employed as a first-principles method for a broad array of real materials⁶⁻⁸, the physical systems ranging from bulk semiconductors¹³ to nanoclusters¹⁴⁻¹⁶ and nanotubes^{17,18}. As the field has advanced, the methodology has been extended to include approximate selfconsistency in the Green's function¹⁹⁻²² and the role of vertex corrections is currently under debate²³⁻²⁵, both at the expense of further computational burden.

Several factors contribute to the complexity of GW-based calculations. The self energy operator is fundamentally non-local and energy dependent. Furthermore, the usual formulation of the calculations for both the screening of the Coulomb interaction and then the electron self energy operator involve a summation over empty states of the reference Hamiltonian. In practical calculations, generation of the corresponding orbitals requires considerably more effort than conventional ground state calculations where the diagonalization can be essentially restricted to the occupied space. Then convergence with respect to the summation over empty states must be carefully checked for each application. Analysis of the algorithms in use shows that the computational burden grows as the fourth power of the system size⁷, although if the short range of the non-locality of some of the operators can be exploited, the scaling improves to essentially quadratic^{7,26}.

Recently there is a resurgence in research directed to improving algorithms so that the GW method can be applied to more complex systems. Proposals have been made for simplified closures of the summation on empty states for the polarizability and self energy operator²⁷. Alternative, efficient basis sets to represent the operators have been explored^{28,29}. Several schemes to reformulate the perturbation theory using iterative techniques³⁰ to avoid explicit calculation of the empty states have been put forward^{31–35}. Although these schemes do not generally alter the scaling with system size, they do show potential for significant changes in the prefactor. This makes the treatment of larger systems feasible in practice.

An alternative approach to simplify the calculations follows the route of physically motivated approximations or models. For example, proposals have been put forward to model the dielectric matrices for solids including local fields^{36,37}. The local approximation to the self energy operator⁹ has been extended to semiconductors through models that incorporate the incomplete screening^{38,39}. The COHSEX approximation of Hedin eliminates the summation over empty states for the self energy operator and has the added benefit of being a static operator, a particular simplification for self consistent calculations^{20,21}. However, the magnitude of the self energy operator is too large, raising concerns for energy level alignment at interfaces, and in application to semiconductors, it tends to substantially overestimate band gaps. One proposal suggested that the dynamical contribution missing in the static COHSEX model could be captured by a linear expansion of the energy dependence in the self-energy and a model dielectric response without extra computational costs⁴⁰. Finally, the hybrid functional approach in DFT, in which a fixed fraction of the exchange opera-

tor based on the bare Coulomb interaction (or a range truncated interaction) is explicitly included, empirically results in improved values for the band gaps in bulk semiconductors and insulators^{41,42}. For the present discussion, this approach can be viewed as an approximation that captures some of the nonlocality of the screened exchange term in the electron self energy. However, the residual does not capture the environment dependence of the screening and hence important physical effects such as the image potential contribution at a surface⁴³. A recently proposed semilocal effective potential approach will likely present similar problems⁴⁴. Overall, previous approaches have been limited in accuracy and in applicability to diverse systems.

A static model for the electron self energy operator offers some compelling advantages, including the orthonormality of the quasiparticle wavefunctions, simplification of a selfconsistent approach and ease of application to more complex systems such as nanoscale junctions. This motivates us to revisit the COHSEX approximation and to investigate the sources of error. Starting with a careful re-examination of the homogeneous electron gases (HEG) case, we find that most of the error comes from the Coulomb-hole (COH) contributions. Physically the error originates from the assumed adiabatic accumulation of the “Coulomb-hole” of the dynamic screened Coulomb interaction. This error is wave-length dependent: it is negligible at long wave-length but introduces a factor of two error at short wave-length. A similar behavior can be seen for the case of crystalline silicon. With this insight, we suggest an empirical model that incorporates a wavelength dependent correction factor to account for the average non-adiabatic effect. Using the results from the HEG as a guide, a simple universal form is proposed for this correction factor, including local field effects in crystals. In this way, we have devised a new approximation which inherits the advantage of efficiency from the static COHSEX approximation but improves its accuracy, as demonstrated for a diverse series of examples. For crystals in particular, we show that the new approximation can be combined with an established model for the dielectric screening³⁷, completely eliminating the sum over empty states from the calculations.

The rest of the article is organized as follows. In Sect. II, the static COHSEX approximation is analyzed. Then in Sect. III, the new method is derived as a natural correction resulting from the analysis. In Sec. IV, the proposed static method is applied to various physical systems. The new results are compared with the static COHSEX approximation and full GW calculation. Section V provides a brief summary.

II. ANALYSIS OF THE COHSEX APPROXIMATION

The electron self energy operator in the GW approximation can be written in the energy domain as

$$\Sigma(\mathbf{r}, \mathbf{r}'; E) = \frac{i}{2\pi} \int dE' e^{-i\delta^+ E'} G(\mathbf{r}, \mathbf{r}'; E - E') W(\mathbf{r}, \mathbf{r}'; E'). \quad (1)$$

where the full one-particle Green's function G and the dynamically screened Coulomb interaction W enter⁵. In most practical calculations the G is replaced by one derived from a reference, single particle Hamiltonian. Often this is based on the Kohn-Sham states calculated with an approximate exchange correlation functional, but it might be derived from an approximate self consistent GW approach, e.g. where the self energy operator is replaced by the COHSEX approximation²⁰ or by the approximate projection in the quasiparticle self consistent approach²¹. With this approximation for G , then the real part of the self energy operator can be easily rewritten in the form

$$\begin{aligned} \Sigma(\mathbf{r}, \mathbf{r}', E) = & - \sum_{n, \mathbf{k}}^{occ} \phi_{n, \mathbf{k}}(\mathbf{r}) \phi_{n, \mathbf{k}}^*(\mathbf{r}') W(\mathbf{r}, \mathbf{r}'; E - E_{n, \mathbf{k}}) \\ & + \sum_{n, \mathbf{k}} \phi_{n, \mathbf{k}}(\mathbf{r}) \phi_{n, \mathbf{k}}^*(\mathbf{r}') P \int_0^\infty dE' \frac{B(\mathbf{r}, \mathbf{r}'; E')}{E - E_{n, \mathbf{k}} - E'}. \end{aligned} \quad (2)$$

The first term is the contribution from the poles of the Green's function G , while the second term comes from the spectral function B of the screened Coulomb interaction W . The symbol P refers to the Cauchy principal value of the integration. The first term is the dynamically screened-exchange (SEX) contribution and the second term is the dynamical Coulomb-hole (COH) contribution⁵.

The static COHSEX approximation can be obtained formally by putting $E - E_{n, \mathbf{k}} \rightarrow 0$ in Eq. (2):

$$\Sigma_{SEX}^{static}(\mathbf{r}, \mathbf{r}', E) = - \sum_{n, \mathbf{k}}^{occ} \phi_{n, \mathbf{k}}(\mathbf{r}) \phi_{n, \mathbf{k}}^*(\mathbf{r}') W(\mathbf{r}, \mathbf{r}'; E = 0), \quad (3)$$

and

$$\Sigma_{COH}^{static}(\mathbf{r}, \mathbf{r}', E) = \frac{1}{2} \delta(\mathbf{r} - \mathbf{r}') W_p(\mathbf{r}, \mathbf{r}'; E = 0), \quad (4)$$

where $W_p = W - v$ and v is the bare Coulomb interaction. Physically, when the self energy operator is evaluated for a specific quasiparticle energy E^{qp} , then the static approximation

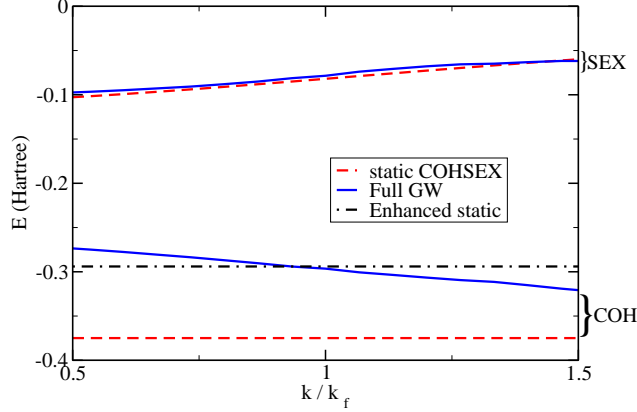


Figure 1: Error analysis of the self energy $\Sigma(k, E_k)$ for the homogeneous electron gas with density parameter $r_s = 2.0$. Here k_f is the magnitude of Fermi wave vector. The Σ is split into COH and SEX contributions, as indicated in the figure. Solid curves are results from full GW calculation, and dashed curves are calculated from the static COHSEX approximation. For references, the COH contribution from the new enhanced static approximation is also displayed in the figure as a dash-dot line.

assumes that the magnitude of the energy $E^{qp} - E_{n,k}$ in Eq. (2) is much smaller than the characteristic energy of the screening, e.g, the plasmon energy¹¹. Alternatively, one can write the approximate formulae in the time domain as

$$\Sigma^{COHSEX}(\mathbf{r}, \mathbf{r}'; t) = iG(\mathbf{r}, \mathbf{r}'; t)[v(\mathbf{r}, \mathbf{r}'; t + \delta^+) + \delta(t)W_p(\mathbf{r}, \mathbf{r}'; E = 0)], \quad (5)$$

where $W_p(\mathbf{r}, \mathbf{r}'; E = 0) = \int_{-\infty}^{+\infty} dt[W(\mathbf{r}, \mathbf{r}'; t) - v(\mathbf{r}, \mathbf{r}'; t)]$. Noting that the $W(\mathbf{r}, \mathbf{r}'; t + \delta^+)$ in the original GW formula can be recast as $W(\mathbf{r}, \mathbf{r}'; t + \delta^+) = v(\mathbf{r}, \mathbf{r}'; t + \delta^+) + [W(\mathbf{r}, \mathbf{r}'; t + \delta^+) - v(\mathbf{r}, \mathbf{r}'; t + \delta^+)]$, it is clear that the only approximation made in the static COHSEX approximation is the substitution of $[W(\mathbf{r}, \mathbf{r}'; t + \delta^+) - v(\mathbf{r}, \mathbf{r}'; t + \delta^+)]$ by $\delta(t)W_p(\mathbf{r}, \mathbf{r}'; E = 0)$. Physically this approximation replaces the time-dependent screened interaction with an instantaneous interaction which is the adiabatic accumulation of the ‘‘Coulomb hole’’ of the time-dependent screened Coulomb interaction^{1,5}.

The adiabatic accumulation of the ‘‘Coulomb hole’’ W_p has different influence on the SEX and COH contributions, although this is difficult to assess analytically. Numerically it can be shown that most of the error in the static COHSEX approximation comes from the COH contribution. The SEX term in the approximation is relatively close to the full GW

calculations. For example, Fig. 1 displays the COH and SEX contributions of the self energy $\Sigma(k, E_k)$, evaluated with the full-frequency Lindhard dielectric function for the homogeneous electron gas of density parameter $r_s = 2.0$. The SEX contribution is around -0.1 Hartree and increases slowly with k . Compared with the full GW calculation, the static COHSEX approximation slightly underestimate the SEX contribution and the difference is less than 5.0×10^{-3} Hartree (0.14 eV) for k from $0.5k_f$ to $1.5k_f$. On the Fermi surface, the difference is 3.4×10^{-3} Hartree (0.093 eV). The COH contribution is independent of k in the static COHSEX approximation, due to the locality in space, while in the full GW calculation, it has modest dispersion. Most striking is the substantial error in the overall magnitude of the COH contribution ranging from 0.10 Hartree (2.7 eV) at $k = 0.5k_f$ to 0.052 Hartree (1.4 eV) at $k = 1.5k_f$. On the Fermi surface the error is 0.078 Hartree (2.1 eV).

Similar trends are also observed in real materials. Table I shows the SEX and COH contributions for bulk Si and LiCl, as well as argon in the solid state, evaluated at the quasiparticle energies of the highest occupied states and the lowest empty states. (For Si, the conduction band minimum is slightly lower, located along the Δ line in the Brillouin zone.) Compared with the results of full GW calculations (described in more detail below in Sect IVA), the static COHSEX approximation has slight deviation for the SEX contributions (up to 0.3 eV), while the magnitude of the COH contributions are overestimated by 1 to 3 eV. For example, the COH contribution to the valence band maximum (VBM) of LiCl, is wrong by 2.6 eV.

To get more insight to the errors, we compare the matrix element of Σ_{COH} for the full GW calculation

$$\langle \mathbf{k} | \Sigma_{COH}^{Full}(E_k) | \mathbf{k} \rangle = \int d\mathbf{q} \left[P \int_0^\infty dE' \frac{B(q, E')}{E_k - E_{q+k} - E'} \right], \quad (6)$$

to that for the static COHSEX approximation

$$\langle \mathbf{k} | \Sigma_{COH}^{static COHSEX}(E_k) | \mathbf{k} \rangle = \int d\mathbf{q} [W_p(q, E = 0)]. \quad (7)$$

Both equations show the wave vector decomposition of the contributions to the COH term. Implicitly, Eq. (6) defines the full accumulation of the ‘‘Coulomb hole,’’ $W_p^{full}(q, E_k)$, the counterpart of $W_p(q, E = 0)$ in Eq. (7). The ratio $f(q, E_k) = \frac{W_p^{full}(q, E_k)}{W_p(q, E=0)}$ reflects the deviation of the adiabatic accumulation at each wave vector \mathbf{q} .

Figure 2 displays typical distributions of $f(q, E_k)$ for the HEG. For small wave vector q (the long wavelength limit), the ratio f approaches to 1, suggesting that the adiabatic

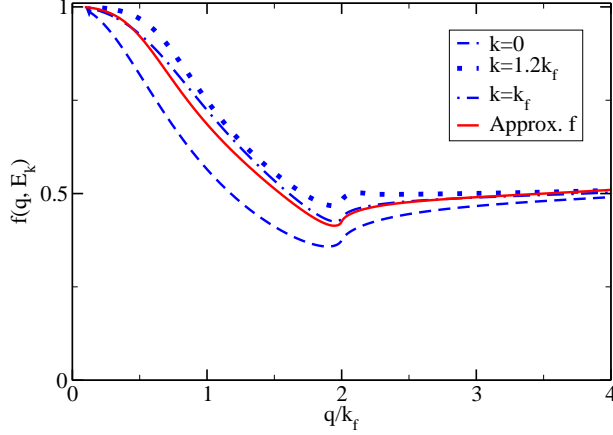


Figure 2: Typical distributions of $f(q, E_k) = \frac{W_p^{full}(q, E_k)}{W_p(q, E=0)}$ of homogeneous electron gas ($r_s=2.0$). The reciprocal of f represents the deviation of the adiabatic accumulation of the “Coulomb hole” W_p as a function of wave vector \mathbf{q} in the static COHSEX approximation. The dotted curve in the figure is the distribution for the state $k = 1.2k_f$, the dash-dot curve is for $k = k_f$, and the dashed curve is for the state $k = 0$. Also displayed in the figure (displayed as a solid curve) is the approximated distribution f^* in Eq. (8) adopted in the new enhanced approximation.

accumulation in the static COHSEX approximation works well. But for large q (the short wavelength limit) the ratio approaches 0.5 asymptotically, which indicates that the adiabatic accumulation exceeds the W_p^{full} by a factor of 2. This large error in the short wavelength limit traces to the fact that screening does not follow the rapid motion of electrons at large q . In between, the ratio f drops smoothly from 1 at $q = 0$ to a value close to 0.5 at $q = 2k_f$; for $q > 2k_f$ the ratio f changes slowly. As seen in Fig. 2, this behavior depends weakly on k . We have also investigated $f(q, E_k)$ for values of density parameter $r_s = 1 - 6$. Provided the wavevector is scaled by the Fermi wavevector, the variation in the curves spans a similar range to the k dependence already shown. While the results in Fig. 2 are based on full numerical calculations in the HEG, the same picture can be derived quite directly from the asymptotic behavior of the Overhauser plasmon pole model⁴⁵. It follows from the fact that as $q \rightarrow 0$ the plasmon frequency ω_q approaches to the classical plasma frequency ω_P , and as $q \rightarrow \infty$ the effective pole frequency ω_q goes to $q^2/2m$.

To probe an example of a semiconductor, the analogous calculation is performed for bulk silicon. In crystals, the screened Coulomb interaction is a function of r and r' separately, not just the difference (as it is in the HEG). For crystals, then W_p and the generalization of

f that we require, are functions defined on discrete points $\mathbf{q} + \mathbf{G}$ and $\mathbf{q} + \mathbf{G}'$, where \mathbf{q} is a wave-vector in the first Brillouin zone, and \mathbf{G} and \mathbf{G}' are reciprocal lattice vectors. In the generalizations of Eqs. (6) and (7) we focus on the contribution of the diagonal elements (where $\mathbf{G} = \mathbf{G}'$) and consider the matrix elements of the self energy operator for the valence band maximum (VBM, Γ'_{25v}) of bulk silicon. The necessary calculations for the screened Coulomb interaction and the GW approximations are performed as described below (Sect. IV). The results are plotted again in the form of a correction factor as a function of $|\mathbf{q} + \mathbf{G}|$ in Fig. 3. The wavevector scale is normalized by $k_{VBM} = \sqrt{\frac{2m}{\hbar^2} \langle \phi_{VBM} | \frac{-\hbar^2 \nabla^2}{2m} | \phi_{VBM} \rangle}$, a simple analog of the Fermi wavevector in the HEG. This effective correction factor shows a similar overall behavior as in the HEG, but at each $|\mathbf{q} + \mathbf{G}|$ point, f can have multiple values. This reflects the orientational anisotropy in real materials. Using k_{VBM} as the scale, the shape of f displayed in Fig. 3 closely resembles that in the HEG.

III. ENHANCED STATIC APPROXIMATION

From the results in Sect. II, a strategy to improve the accuracy emerges: simply include a correction factor to the adiabatic $W_p(E = 0)$ in Eq.(4). Ideally, the factor is just the wavevector resolved and energy dependent ratio $f(q, E_k)$. However, the results of Fig. 2 suggest that the density and the k or E_k dependence of the correction factor is not large, except for the scaling of the wavevector q . Furthermore, the possibility to drop the E_k dependence results in an energy independent (static) model for the self energy operator. Therefore a universal function f^* is proposed. A convenient Pade form for f^* is chosen and fit to the $f(q, E_f)$ for HEG of $r_s=1.0$:

$$f^*(x) = \frac{1 + 1.9085x - 0.542572x^2 - 2.45811x^3 + 3.08067x^4 - 1.806x^5 + 0.410031x^6}{1 + 2.01317x - 1.55088x^2 + 1.58466x^3 + 0.368325x^4 - 1.68927x^5 + 0.599225x^6}, \quad (8)$$

where x represents the dimensionless wave number q/k_f . It is also displayed as the solid curve in Fig. 2.

For the HEG, the enhanced static approximation retains the usual static screened interaction term and alters the Coulomb hole term:

$$\Sigma_{COH}^{new} = \frac{1}{2} \delta(\mathbf{r} - \mathbf{r}') \int d\mathbf{q} e^{-i\mathbf{q} \cdot \mathbf{r}} W_p(q, E = 0) f^*(q/k_f). \quad (9)$$

		GW		COHSEX		New Static	
		Σ_{SEX}	Σ_{COH}	Σ_{SEX}	Σ_{COH}	Σ_{SEX}	Σ_{COH}
Si	Γ'_{25v}	-3.83	-8.28	-3.91	-10.43	-3.91	-8.21
(bulk)	X_{1c}	-1.74	-7.40	-2.06	-8.72	-2.06	-7.25
LiCl	Γ_{15v}	-8.59	-8.24	-8.69	-10.84	-8.69	-7.91
(bulk)	Γ_{1c}	-1.90	-6.34	-2.25	-7.06	-2.25	-5.76
Ar	Γ_{15v}	-12.77	-7.24	-12.79	-10.07	-12.79	-6.91
(bulk)	Γ_{1c}	-1.24	-4.01	-1.56	-4.25	-1.56	-3.55

Table I: The SEX and COH contributions to the matrix elements of the self energy Σ for states that define the energy gap for bulk silicon, bulk lithium chloride, and argon in its solid phase, all in eV. Results from the full GW (with the GPP model), the static COHSEX approximation, and the new enhanced static approximations are presented. The self energies in the full GW calculations are evaluated at the corresponding quasiparticle energies.

The improvement of the new approximation is easy to verify for the HEG, as illustrated in Fig. 1 for $r_s = 2.0$. The error from the COH contribution decreases to 0.07 eV from 2.1 eV at the Fermi surface. Examining the range $r_s = 1 - 6$, the error remains within 0.2 eV at the Fermi surface. That range of r_s represents typical electronic densities in most bulk materials. Since this static approximation to the Coulomb hole term remains local in space, it has no dispersion, as seen in Fig.1. The occupied bandwidth will still be overestimated in this new static approximation.

In order to extend this idea to real materials, two factors must be addressed. First a systematic scheme to derive a wavevector scale is required. We choose the scale $k_{VBM} = \sqrt{\frac{2m}{\hbar^2} \langle \phi_{VBM} | \frac{-\hbar^2 \nabla^2}{2m} | \phi_{VBM} \rangle}$ where ϕ_{VBM} refers to the highest occupied electronic state in the system. In the limit of the HEG, k_{VBM} goes back to k_f , so it is a reasonable generalization. With this scale factor the approximate f^* , the solid curve in Fig. 3, is still a good description of the diagonal terms in the numerically calculated corrections.

Second, the effect of local fields must be incorporated into the correction factor f . We have tested several different generalizations that preserve symmetry and reduce back to the

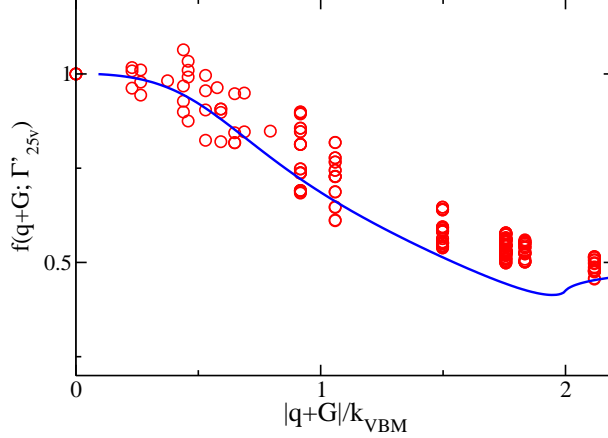


Figure 3: Diagonal elements of the ratio $f(\mathbf{q} + \mathbf{G}, \mathbf{q} + \mathbf{G}'; \Gamma'_{25v})$ at the valence band maximum of bulk silicon as a function of $|\mathbf{q} + \mathbf{G}|$, displayed as circles in the figure. The solid curve is the approximate f^* specified in Eq. (8), and k_{VBM} is the characteristic wave number scale derived from the average speed of electrons at the highest occupied electronic state of the system.

simple form for the HEG limit. We find that a simple ansatz where f^* is only a function of $\sqrt{|\mathbf{q} + \mathbf{G}||\mathbf{q} + \mathbf{G}'|}/k_{VBM}$ works well in practice. Accordingly the new static approximation for the COH term is revised to be

$$\Sigma_{COH}^{new}(\mathbf{r}, \mathbf{r}') = \frac{1}{2} \delta(\mathbf{r} - \mathbf{r}') \sum_{\mathbf{q}, \mathbf{G}, \mathbf{G}'} e^{-i(\mathbf{q} + \mathbf{G}') \cdot \mathbf{r}'} e^{i(\mathbf{q} + \mathbf{G}) \cdot \mathbf{r}} W_{p, \mathbf{G}, \mathbf{G}'}(\mathbf{q}, E = 0) f^* \left(\frac{\sqrt{|\mathbf{q} + \mathbf{G}||\mathbf{q} + \mathbf{G}'|}}{k_{VBM}} \right). \quad (10)$$

Note that the f^* used here is exactly the same as the one defined in Eq. (8). The f^* in real materials should generally be a function of both $\mathbf{q} + \mathbf{G}$ and $\mathbf{q} + \mathbf{G}'$ separately. Our simple ansatz is isotropic and only depends on the amplitudes of $\mathbf{q} + \mathbf{G}$ and $\mathbf{q} + \mathbf{G}'$.

IV. RESULTS

In order to test the proposed new static approximation, calculations are performed for a diverse set of examples including crystals, molecules, atoms and a carbon nanotube. All calculations are performed with geometrical parameters obtained from experiments. All the LDA calculations are carried out in a plane-wave basis using the Quantum Espresso package⁴⁶ with norm conserving pseudopotentials generated by the FHI99P packages⁴⁷ using the Troullier-Martins method⁴⁸. The pseudopotentials are taken from the website of

	Si	C	LiCl	GaAs	Ar
a_0 (nm)	0.543 ^a	0.357 ^a	0.513 ^b	0.565 ^b	0.531 ^a
ϵ_∞	12.0 ^c	5.5 ^c	2.7 ^b	10.9 ^b	1.6 ^d

^aRef. 51

^bRef. 52

^cRef. 53

^dRef. 54

Table II: Experimental lattice constants a_0 and macroscopic dielectric constants ϵ_∞ of the bulk materials calculated, where ϵ_∞ are parameters required by the model dielectric matrices³⁷.

ABINIT^{49,50}. In the full GW calculations, the GPP model is used¹¹. Only the first order energy correction to the diagonal elements are calculated. No further updates of spectra are included in the calculations. The new static approximation is applied with the same statically screened Coulomb interaction used in the full GW calculations. For several bulk materials, the fundamental gaps are also calculated using model dielectric matrices to obtain the statically screened Coulomb interactions³⁷. This approach completely eliminates any explicit summations on empty states in the calculation.

For all the bulk materials (including Si, C, solid Ar, GaAs, and LiCl), the LDA wavefunctions and eigenvalues are calculated with 80 Ry energy cutoff and the Brillouin zone is sampled by a $4 \times 4 \times 4$ Monkhorst-Pack (MP) mesh⁵⁵. Their lattice constants are listed in Table II together with macroscopic dielectric constants required by the model dielectric matrices.³⁷ In the GW calculations, the screened and unscreened Coulomb interaction are cut off at 40 Ry. 160 bands are used for the calculation of Green's function and the screened Coulomb interaction. In the calculations of atoms and molecules (including benzene, methene, and argon atom), the LDA wavefunctions and eigenvalues are calculated with 50 Ry energy cutoff in a cubic computational cell of 1.323 nm (25.0 Bohr) for each side. In the GW calculations, the unscreened Coulomb interaction is cut off at 10 Ry, while the screened Coulomb interaction is cut off at 6 Ry. 700 LDA bands are used for the calculation of the Green's functions and screened Coulomb interaction. The LDA wavefunctions and eigenvalues of the single-wall carbon nanotube (SWCNT) (8, 0) is calculated in a trigonal computational cell of $a = 2.381$ nm (45.0 Bohr) and $c = 0.421$ nm (7.956 Bohr). The energy cutoff for the LDA wavefunction is 60 Ry and the Brillouin zone is sampled by a $1 \times 1 \times 8$ MP

grid. The unscreened Coulomb interaction is cut off at 20 Ry. A cutoff of 6 Ry and 1000 bands are used to calculate the screened Coulomb interaction and Green's function. With the choice of above computational parameters, the GW energy gap are expected to converge within 0.1 eV for bulk materials and within 0.2 eV for other systems. For the SWCNT system, our computational parameters are slightly different from the previous calculation¹⁷. In particular, we do not enforce a cut off of the Coulomb interaction in the radial direction to eliminate screening from tubes in neighboring cells. This reduces computational costs. Our results including that extra screening lead to a smaller quasiparticle energy gap, but the test of the new static method here is done with the same approximation.

Silicon in the diamond structure is the prototypical covalent semiconductor crystal and a standard test case. Since its quasiparticle wavefunctions and charge density are extended to fill the entire volume, it is often considered as an inhomogeneous electron gas with an energy gap in a simplified model⁵⁶. The quasiparticle energies calculated using the new enhanced static approximation, the static COHSEX approximation and the full GW calculation are summarized in Table III together with experimental observations. The differences with the previous results¹¹ in the full GW calculations come partly from higher cut-offs in the present calculation and also because no update of the spectrum is included here. Relative to the valence band edge, the lowest energy conduction band states at the Γ , X and L points of the Brillouin zone are all remarkably similar to the full GW results. By comparison, the static COHSEX approximation places these states 0.4-0.7 eV higher in energy than the full GW results. The minimum band gap, involving the lowest conduction band along the Δ line at about 85% of the distance to the X point is estimated with the new method to be 1.18 eV, slightly smaller than the full GW result 1.32 eV, closely following the result at the X point. The results based on the new method for all the low lying empty states are in good agreement with experiment (about 0.1 eV or better). Turning to the occupied states, the new method predicts quasiparticle energies that are systematically deeper than the full GW calculations, by an amount that increases further from the valence band edge. At the bottom of the valence band, the Γ_{1v} quasiparticle energy calculated using the new method is -13.08 eV, 1.33 eV lower than the full GW results and deeper than experiment. This is not surprising, since the accuracy of the new method is optimized for bands near the Fermi energy and the trend illustrated in Fig.1 for the homogeneous electron gas also holds here. Referring to Table I, the final results with the new method clearly benefit from

Si	LDA	COHSEX	GW	New Static	Expt.
Γ_{1v}	-11.97	-12.81	-11.74	-13.08	-12.5 \pm 0.6
Γ'_{25v}	0	0	0	0	
Γ_{15c}	2.56	3.86	3.35	3.45	3.4
Γ'_{2c}	3.11	4.24	3.86	4.17	4.2
L'_{2v}	-9.63	-10.35	-9.57	-10.50	-9.3 \pm 0.4
L_{1v}	-6.99	-7.26	-6.98	-7.61	-6.7 \pm 0.2
L'_{3v}	-1.19	-1.20	-1.21	-1.29	-1.2 \pm 0.2,1.5
L_{1c}	1.42	2.61	2.18	2.24	2.1,2.4 \pm 0.15
L_{3c}	3.33	4.77	4.21	4.23	4.15 \pm 0.1
L'_{2c}	7.55	9.50	8.37	8.40	
X_{1v}	-7.82	-8.37	-7.84	-8.51	
X_{4v}	-2.85	-2.86	-2.86	-3.10	-2.9,-3.3 \pm 0.2
X_{1c}	0.64	2.05	1.46	1.31	1.3
X_{4c}	9.96	11.58	10.67	11.37	

Table III: Quasiparticle energies of crystalline Si calculated with different methods. Here “COHSEX” refers to the static COHSEX approximation, “GW” refers to full GW results with a generalized plasmon-pole model, and “New Static” refers to the results from the new enhanced static approximation. Experimental results are quoted from Ref. 11. All energies in the table are presented in eV.

some cancellation of errors between the SEX and COH terms. Also, relevant for energy level alignment at interfaces, the magnitude of the self energy at the valence band edge is -12.11 eV in the full GW calculation, -14.34 eV for the static COHSEX and -12.12 eV for the new model. The error for the new model is just 0.01 as compared to 2.2 eV for COHSEX.

Lithium chloride (LiCl) is a typical ionic crystal with a rock salt structure. Unlike silicon, the charge density and quasiparticle wave functions of LiCl are localized around Cl^- anions

and Li^+ cations. Since the system is conceptually far from an extended electron gas, it raises a challenge for the new method originally derived from a HEG model. The fundamental band gap calculated using the new method is 8.98 eV, very close to the full GW calculation and 1.6 eV smaller than the static COHSEX result (Table IV). Like the full GW result, the calculated value is about 0.4 eV smaller than the measured value, as was observed in the previous full GW calculations⁵⁷. The placement of the empty bands at the high symmetry points of the Brillouin zone shows an accuracy, relative to the full GW calculations, similar to the case of Si. Also, very similar to the Si case, the new method is systematically places the occupied states too deep. As illustrated in Table I, the deviations for the individual SEX and COH terms are larger. The net error in the absolute magnitude of the valence band matrix element of the self energy operator is modest (0.3 eV), especially as compared to the COHSEX approximation (2.7 eV).

Solid argon presents a third type of solid, with a large band gap related to the underlying energy gap between the occupied 3p shell and the empty 4s and 4p derived bands. The new method gives a calculated minimum band gap within 0.2 eV of the full GW result, in contrast to the COHSEX derived gap, which is 2.3 eV larger (Table IV). Other trends are similar. In particular, there is modest cancellation between errors in the separate SEX and COH terms (Table I). The net error in the valence band edge matrix element of the self energy operator is about 0.3 eV, as compared to the 2.9 eV error in the COHSEX approximation.

In Fig. 4 and Table IV the fundamental gaps calculated using the new static method are compared with full GW calculations for different types of materials including Si (diamond structure), C (diamond), LiCl crystal, GaAs crystal, Ar (solid), Ar (atom), benzene (molecule), methane (molecule), and single wall carbon nanotube SWCNT(8, 0). Both calculations are based on the same LDA wavefunctions and eigenstates. The choices of materials in the figure cover fundamental gaps from around 1 eV up to 15 eV, and they represent atoms, molecules, nanostructures, and various bulk materials. As indicated in the figure, all the diamond points (which represent results from the new method) tightly follow the diagonal line, showing very good accuracy, about 10% or better. The largest relative errors are seen for bulk Si and the SWCNT cases. For several bulk materials (Si, C, LiCl, GaAs, and solid Ar), we also show the results from the combination of our new method and a model dielectric matrix³⁷ aimed to further speed up the calculation. The results are displayed as squares in the figure, showing that the accuracy is still maintained.

	LDA	COHSEX	GW	New Static	Notes
Si(bulk)	2.56	3.86	3.35	3.45	$E_g^{\Gamma, Direct}$
	0.49	1.91	1.32	1.18 (1.06)	$E_g^{Indirect}$
C(diamond)	5.56	8.35	7.56	8.00 (7.72)	$E_g^{\Gamma, Direct}$
	4.20	6.99	5.70	5.93 (5.57)	$E_g^{Indirect}$
LiCl(bulk)	5.91	10.61	8.99	8.98 (9.24)	E_g
GaAs(bulk) ^a	0.40	1.43	1.12	1.17 (1.17)	E_g
Ar(bulk)	8.12	15.85	13.56	13.40 (14.15)	E_g
Ar (atom)	9.99	16.25	14.80	14.79	HO/LU
Benzene	5.22	11.50	10.71	11.43	HO/LU
Methane	9.01	15.21	13.54	13.96	HO/LU
SWCNT80	0.61	1.78	1.51	1.73	E_g

^aA spin-orbital splitting correction¹³ of 0.11 eV is included on the first order perturbation level.

Table IV: Energy gap of a variety of materials calculated using the different methods as described at the beginning of Sec. IV. All the energies in the table are presented in eV. Values appearing in parenthesis in the "New Static" column are calculated with a model dielectric matrix as described in the text. The character of the gap is noted in the final column where the notation "HO/LU" refers to the gap between the highest occupied molecular orbital and the lowest unoccupied molecular orbital.

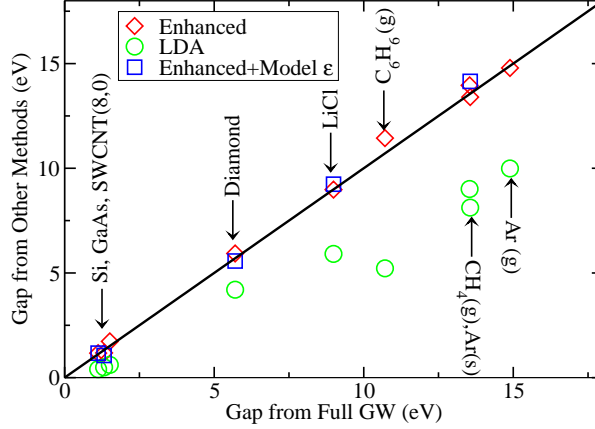


Figure 4: Fundamental gaps of different physical systems compared with values calculated from full GW method. Diamonds are gaps from the new enhanced static approximation, squares are from a method combining the new method and a model dielectric matrix³⁷, and circles are gaps from the LDA calculation.

Two examples specifically probe a pi-electron gap, the case of the gas-phase benzene and the (8, 0) SWCNT. In this case, the new static method and the COHSEX method give essentially the same results. In turn, the difference between the COHSEX results and those from the full GW calculation in these cases is much more modest than for the other cases: about 0.7 eV for benzene and 0.2 eV for the SWCNT. A closer examination of the full GW calculations show that in this instance the contribution of the COH term to the band gap is quite small. This is quite different from the situation for other systems considered here. For example, in the methane molecule, the COHSEX approximation gives a gap that is too large by about 1.7 eV, while the new method provides a gap that is within 0.4 eV.

V. SUMMARY

A static approximation to the electron self energy offers several technical advantages, not least of which is to maintain a hermitian operator in the calculation of quasiparticle energies. In addition, it offers the potential to avoid the computational burden of converging the sum over empty states that dominates the full application of many-body perturbation theory. Here we have analyzed the original static COHSEX approximation proposed by Hedin, showing that most of the errors trace to the assumption of an adiabatic accumulation of the Coulomb hole in the short wavelength limit. This has lead us to propose a simple

generalization in which a single function of the scaled internal momentum in the Coulomb hole term is used to correct this error. Although it requires an additional ansatz to represent the local fields, this simple, enhanced static approximation goes a surprisingly long way to correct the errors of the original COHSEX approximation for application to diverse real materials, ranging from crystals and nanotubes to molecules and atoms. The accuracy of the new approximation may be sufficient for a number of applications to larger scale systems. It may also provide an efficient approximate approach for self consistent calculations.

Acknowledgments

Work performed under the auspices of the U.S. Department of Energy under Contract No. DEAC02-98CH1-886. This research utilized resources at the New York Center for Computational Sciences at Stony Brook University/Brookhaven National Laboratory which is supported by the U.S. Department of Energy under Contract No. DE-AC02-98CH10886 and by the State of New York.

-
- ¹ L. Hedin and S. Lundqvist, Solid State Phys. **23**, 1 (1969).
 - ² P. Hohenberg and W. Kohn, Phys. Rev. **136**, B864 (1964).
 - ³ W. Kohn and L. J. Sham, Phys. Rev. **140**, A1133 (1965).
 - ⁴ R. O. Jones and O. Gunnarsson, Rev. Mod. Phys. **61**, 689 (1989).
 - ⁵ L. Hedin, Phys. Rev. **139**, A796 (1965).
 - ⁶ F. Aryasetiawan and O. Gunnarsson, Rep. Prog. Phys. **61**, 237 (1998).
 - ⁷ W. G. Aulbur, L. Jönsson, and J. W. Wilkins, Solid State Phys. **54**, 1 (1999).
 - ⁸ G. Onida, L. Reining, and A. Rubio, Rev. Mod. Phys. **74**, 601 (2002).
 - ⁹ L. J. Sham and W. Kohn, Phys. Rev. **145**, 561 (1966).
 - ¹⁰ M. S. Hybertsen and S. G. Louie, Phys. Rev. Lett. **55**, 1418 (1985).
 - ¹¹ M. S. Hybertsen and S. G. Louie, Phys. Rev. B **34**, 5390 (1986).
 - ¹² R. W. Godby, M. Schlüter, and L. J. Sham, Phys. Rev. B **35**, 4170 (1987).
 - ¹³ X. Zhu and S. G. Louie, Phys. Rev. B **43**, 14142 (1991).
 - ¹⁴ S. Saito, S. B. Zhang, S. G. Louie, and M. L. Cohen, Phys. Rev. B **40**, 3643 (1989).

- ¹⁵ G. Onida, L. Reining, R. W. Godby, R. Del Sole, and W. Andreoni, Phys. Rev. Lett. **75**, 818 (1995).
- ¹⁶ L. Reining, O. Pulci, M. Palummo, and G. Onida, Int. J. Quantum Chem. **77**, 951 (2000).
- ¹⁷ C. Spataru, S. Ismail-Beigi, L. Benedict, and S. Louie, Appl. Phys. A **78**, 1129 (2004).
- ¹⁸ T. Miyake and S. Saito, Phys. Rev. B **72**, 073404 (2005).
- ¹⁹ W. Ku and A. G. Eguiluz, Phys. Rev. Lett. **89**, 126401 (2002).
- ²⁰ F. Bruneval, N. Vast, and L. Reining, Phys. Rev. B **74**, 045102 (2006).
- ²¹ T. Kotani, M. van Schilfgaarde, and S. V. Faleev, Phys. Rev. B **76**, 165106 (2007).
- ²² M. Shishkin and G. Kresse, Phys. Rev. B **75**, 235102 (2007).
- ²³ E. L. Shirley, Phys. Rev. B **54**, 7758 (1996).
- ²⁴ B. Holm and U. von Barth, Phys. Rev. B **57**, 2108 (1998).
- ²⁵ M. Shishkin, M. Marsman, and G. Kresse, Phys. Rev. Lett. **99**, 246403 (2007).
- ²⁶ M. M. Rieger, L. Steinbeck, I. D. White, H. N. Rojas, and R. W. Godby, Comput. Phys. Commun. **117**, 211 (1999).
- ²⁷ F. Bruneval and X. Gonze, Phys. Rev. B **78**, 085125 (2008).
- ²⁸ D. Lu, F. Gygi, and G. Galli, Phys. Rev. Lett. **100**, 147601 (2008).
- ²⁹ P. Umari, G. Stenuit, and S. Baroni, Phys. Rev. B **79**, 201104 (2009).
- ³⁰ S. Baroni, S. de Gironcoli, A. Dal Corso, and P. Giannozzi, Rev. Mod. Phys. **73**, 515 (2001).
- ³¹ H. F. Wilson, F. Gygi, and G. Galli, Phys. Rev. B **78**, 113303 (2008).
- ³² H. F. Wilson, D. Lu, F. Gygi, and G. Galli, Phys. Rev. B **79**, 245106 (2009).
- ³³ H.-V. Nguyen and S. de Gironcoli, Phys. Rev. B **79**, 205114 (2009).
- ³⁴ P. Umari, G. Stenuit, and S. Baroni, Phys. Rev. B **81**, 115104 (2010).
- ³⁵ F. Giustino, M. L. Cohen, and S. G. Louie, Phys. Rev. B **81**, 115105 (2010).
- ³⁶ M. Ortuno and J. C. Inkson, J. Phys. C **12**, 1065 (1979).
- ³⁷ M. S. Hybertsen and S. G. Louie, Phys. Rev. B **37**, 2733 (1988).
- ³⁸ C. S. Wang and W. E. Pickett, Phys. Rev. Lett. **51**, 597 (1983).
- ³⁹ F. Gygi and A. Baldereschi, Phys. Rev. Lett. **62**, 2160 (1989).
- ⁴⁰ F. Bechstedt, R. D. Sole, G. Cappellini, and L. Reining, Solid State Commun. **84**, 765 (1992).
- ⁴¹ J. Muscat, A. Wander, and N. M. Harrison, Chem. Phys. Lett. **342**, 397 (2001).
- ⁴² J. Heyd, J. E. Peralta, G. E. Scuseria, and R. L. Martin, J. Chem. Phys. **123**, 174101 (2005).
- ⁴³ J. B. Neaton, M. S. Hybertsen, and S. G. Louie, Phys. Rev. Lett. **97**, 216405 (2006).

- ⁴⁴ F. Tran and P. Blaha, Phys. Rev. Lett. **102**, 226401 (2009).
- ⁴⁵ A. W. Overhauser, Phys. Rev. B **3**, 1888 (1971).
- ⁴⁶ P. Giannozzi, S. Baroni, N. Bonini, M. Calandra, R. Car, C. Cavazzoni, D. Ceresoli, G. L. Chiarotti, M. Cococcioni, I. Dabo, et al., J. Phys.: Condens. Matter **21** (2009).
- ⁴⁷ M. Fuchs and M. Scheffler, Comput. Phys. Commun. **119**, 67 (1999).
- ⁴⁸ N. Troullier and J. L. Martins, Phys. Rev. B **43**, 1993 (1991).
- ⁴⁹ X. Gonze, J. M. Beuken, R. Caracas, F. Detraux, M. Fuchs, G. M. Rignanese, L. Sindic, M. Verstraete, G. Zerah, F. Jollet, et al., Comput. Mater. Sci. **25**, 478 (2002).
- ⁵⁰ X. Gonze, G. M. Rignanese, M. Verstraete, J. M. Beuken, Y. Pouillon, R. Caracas, F. Jollet, M. Torrent, G. Zerah, M. Mikami, et al., Zeitschrift Fur Kristallographie **220**, 558 (2005).
- ⁵¹ C. Kittel, *Introduction to Solid State Physics* (John Wiley & Sons, 1996), 7th ed.
- ⁵² U. Madelung, M. Schulz, H. Weiss, and Landolt-Bornstein, eds., *Zahlenwerte und Funktionen aus Naturwissenschaften und Technik*, vol. 3, Pt. 17a and 22a of *New Series* (Springer-Verlag, Berlin, 1982), as cited in Ref. 13.
- ⁵³ O. Madelung, M. Schulz, H. Weiss, and Landolt-Bornstein, eds., *Semiconductors*, vol. 17a of *Group 3* (Springer, Berlin, 1982), as cited in Ref. 37.
- ⁵⁴ I. Lefkowitz, K. Kramer, M. A. Shields, and G. L. Pollack, J. Appl. Phys. **38**, 4867 (1967).
- ⁵⁵ H. J. Monkhorst and J. D. Pack, Phys. Rev. B **13**, 5188 (1976).
- ⁵⁶ Z. H. Levine and S. G. Louie, Phys. Rev. B **25**, 6310 (1982).
- ⁵⁷ M. S. Hybertsen and S. G. Louie, Phys. Rev. B **32**, 7005 (1985).